Biomaterials 40 (2015) 12–22

Contents lists available at ScienceDirect

Biomaterials

journal homepage: www.elsevier.com/locate/biomaterials

Graphene oxide as a chemosensitizer: Diverted autophagic flux, enhanced nuclear import, elevated necrosis and improved antitumor effects

Guan-Yu Chen [a, 1], Chia-Le Meng [a, 1], Kuan-Chen Lin [a, b], Hsing-Yu Tuan [a], Hong-Jie Yang [a], Chiu-Ling Chen [a], Kuei-Chang Li [a], Chi-Shiun Chiang [b], Yu-Chen Hu [a, *]

[a] Department of Chemical Engineering, National Tsing Hua University, Hsinchu 300, Taiwan
[b] Department of Biomedical Engineering and Environmental Sciences, National Tsing Hua University, Hsinchu 300, Taiwan

ARTICLE INFO

Article history:
Received 15 August 2014
Accepted 7 November 2014
Available online 29 November 2014

Keywords:
Autophagy
Cisplatin
Chemoresistance
Graphene oxide
Nuclear import
Necrosis

ABSTRACT

Graphene oxide (GO) is a nanomaterial that provokes autophagy in CT26 colon cancer cells and confers antitumor effects. Here we demonstrated that both GO and the chemotherapy drug cisplatin (CDDP) induced autophagy but elicited low degrees of CT26 cell death. Strikingly, GO combined with CDDP (GO/CDDP) potentiated the CT26 cell killing via necrosis. GO/CDDP not only elicited autophagy, but induced the nuclear import of CDDP and the autophagy marker LC3. The nuclear LC3 did not co-localize with p62 or Lamp-2, neither did blocking autolysosome formation significantly hinder the nuclear import of LC3/CDDP and necrosis, indicating that autophagosome and autolysosome formation was dispensable. Conversely, suppressing phagophore formation and importin-α/β significantly alleviated the nuclear import of LC3/CDDP and necrosis. These data suggested that GO/CDDP diverted the LC3 flux in the early phase of autophagy, resulting in LC3 trafficking towards the nucleus in an importin-α/β-dependent manner, which concurred with the CDDP nuclear import and necrosis. Intratumoral injection of GO/CDDP into mice bearing CT26 colon tumors potentiated immune cell infiltration and promoted cell death, autophagy and HMGB1 release, thereby synergistically augmenting the antitumor effects. Altogether, we unveiled a mechanism concerning how nanomaterials chemosensitize cancer cells and demonstrated the potentials of GO as a chemosensitizer.

1. Introduction

Macroautophagy (henceforth referred to as autophagy) is a cellular process by which cytoplasmic materials are delivered to lysosomes for degradation [1]. Autophagy induction through the inhibition of mammalian target of rapamycin (mTOR) results in translocation of the mTOR substrate complex from the cytosol to the endoplasmic reticulum (ER). This leads to the recruitment of class III phosphatidylinositol-3-OH kinase (PI(3)K) complex to the ER and induces the formation of phagophore. Ensuing phagophore elongation, autophagosome formation and engulfment of cytoplasmic materials involve multiple proteins. For instance, microtubule-associated light chain 3 (LC3) plays roles in the completion of autophagosome formation, during which lipid conjugation converts LC3 from the soluble form (LC3-I) to the form attached to the phagophore membrane (LC3-II). The adaptor protein p62 interacts with polyubiquitinated targets and the p62-cargo complex is selectively tethered to autophagosomes by the interaction of p62 and LC3. At the late stage, autophagosomes undergo fusion with lysosomes to form autolysosomes, which is mediated by a receptor in the lysosomal membrane, the lysosome-associated membrane protein 2 (Lamp-2). In the autolysosomes, the lumenal cargo is degraded by lysosomal enzymes (for review see Refs. [1–3]). Autophagy is frequently activated in cancer cells in response to chemotherapy [2]. Although the roles of autophagy in cancer therapy remain elusive, it is known that autophagy has two primary and opposing functions in tumor cells in response to

* Corresponding author. Tel.: +886 3 571 8245; fax: +886 3 571 5408.
E-mail address: ychu@mx.nthu.edu.tw (Y.-C. Hu).
[1] These two authors contributed equally to this work.

http://dx.doi.org/10.1016/j.biomaterials.2014.11.034
0142-9612/

chemotherapy. One is the cytoprotective function that enables cells to survive the stress; the other is the cytotoxic function that may promote tumor cell killing [4].

Graphene oxide (GO) is a derivative of graphene and has drawn intense attention for many bioapplications including cellular growth and differentiation [5] gene and drug delivery [6,7] and photothermal therapy [8,9]. GO can simultaneously activate toll-like receptor (TLR)-4 and -9 responses as well as autophagy in macrophages [10] and colon cancer cell CT26 [11]. Furthermore, injection of GO alone stimulates the immune cell infiltration into the tumor bed and inhibits colon cancer growth in mice [11].

Chemotherapy is one of the cancer therapy modalities and numerous drugs such as irinotecan (CPT-11), doxorubicin (DOX), oxaliplatin (OXA) and cisplatin (CDDP) have been used for chemotherapy [12,13]. Treatment of colon cancer cells with CPT-11 (10–50 μg/mL), CDDP (100 μg/mL), OXA (5–120 μg/mL) or DOX (2–10 μg/mL) for 24 h can cause cell death [14–16]. However, a variety of tumor and cancer cell types have evolved resistance to chemotherapy drugs, thus entailing the need of new drugs or combination therapies to overcome the chemoresistance. In this regard, nanomaterials such as fullerene C60 nanocrystal (Nano-C60) may be a new chemosensitizer, because CDDP at 10 μg/mL only kills 6.3% of HeLa cells but combination of CDDP with Nano-60 greatly enhances the killing of HeLa cells to 34.2% [17]. Such chemosensitization depends on autophagy induced by Nano-60, but the underlying mechanism remains unknown [17]. Also, GO conjugated with chemotherapy drugs (DOX and CPT-11) can enhance the killing of MCF-7 cells that are resistant to DOX and CPT [7].

Given that autophagy may attenuate the chemoresistance of cancer cells [7,17] and GO is a potent autophagy inducer in colon cancer cell CT26, we were inspired to explore whether GO can act in concert with chemotherapy drugs to overcome the chemoresistance, enhance the CT26 cell killing and ameliorate colon cancer treatment. We first evaluated which combination of GO and chemotherapy drug enhanced the killing of CT26 cells and explored the death mechanism. We next examined the correlation of cell death, autophagy and intracellular trafficking after treatment with GO and the drug. Finally, we assessed the antitumor effects after co-injection of GO and the drug into immunocompetent mice bearing CT26 tumors.

2. Materials and methods

2.1. Cell culture

Mouse colorectal carcinoma cell CT26 (ATCC CRL-2638) was routinely cultured and passaged in T75 flasks at 37 °C and 5% CO_2, using RPMI-1640 medium (Gibco) supplemented with 10% fetal bovine serum (FBS, Biological Industries) and 1% antibiotics (PEN-STREP-AMPHO SOL, Biological Industries).

2.2. Preparation of GO nanosheets and chemotherapy drug stock solutions

The GO nanosheets (thickness<2 nm) with characteristic functional groups and a lateral size of ≈450 nm in mean diameter (size range≈100–800 nm) were prepared and characterized as described previously [10] and dispersed in water at 250 μg/mL as the stock solution. To determine the subcellular distribution, GO was labeled with rhodamine 6G (R6G) as described previously [18,19] and dispersed in water (250 μg/mL). The chemotherapy drugs CPT-11 (Sigma) and CDDP (Millipore) were dissolved in dimethyl sulfoxide (DMSO) at 50 and 25 mg/mL, respectively. DOX (Millipore) and OXA (Sigma) were dissolved in water at 10 and 5 mg/mL, respectively.

2.3. Treatment of cells with GO and chemotherapy drugs

For all treatments, CT26 cells were seeded to 6-well plates (3×10^5 cells/well), 12-well plates (1.5×10^5 cells/well) or 10 cm plates (1.8×10^6 cells/dish) overnight. For GO treatment, the GO stock solution (250 μg/mL) was mixed with equal volume of concentrated complete medium (2×), and further diluted to 50 μg/mL by mixing with complete RPMI-1640 medium (1×). After PBS washes, the cells were treated with GO (50 μg/mL) by culturing in the GO-containing medium for 24 h. For chemotherapy drug treatment, the drug stock solution was added to the complete RPMI-1640 medium containing 10% FBS (1×) to the final concentration (see Results) and the cells were cultured in the drug-containing medium for 24 h. For co-treatment with GO and the drug, the drug stock solution was added to the GO-containing medium to the final concentration (see Results) and the cells were cultured for 24 h. For the untreated control, the cells were simply cultured using the complete medium (1×) for 24 h.

For pretreatment with inhibitors, CT26 cells were cultured in 6-well plates overnight and the inhibitor stock solution was directly added to the RPMI-1640 medium to final concentrations (1 mM for 3-MA; 50 nM for BafA1; 50 μM for IVM; 100 μM for Nec-1). As the control, DMSO used for dissolving CDDP was added to the medium (20 μg/mL). After gentle shaking, the cells were incubated at 37 °C for 1 h (for DMSO, BafA1, IVM and Nec-1) or 12 h (for 3-MA). After PBS washes, the cells were co-treated with GO/CDDP as described above.

2.4. Cell death analyses

CT26 cells cultured in 12-well plates were treated with chemotherapy drugs with or without GO as described above. After 24 h incubation, the cell viability was evaluated by MTT (3-[4,5-dimethylthiazol-2-yl]-2,5-diphenyltetrazolium bromide, Sigma) assays. Alternatively, the cells cultured in 6-well plates were co-treated with GO/CDDP for 24 h as described above. Apoptosis and necrosis were quantified by two-dimensional flow cytometry, using the PE Annexin V/7 amino-actinomycin (7-AAD) Apoptosis Detection Kit I (BD Biosciences).

2.5. Immunofluorescence microscopy and analysis

CT26 cells were seeded to coverslips in the 6-well plates (3.0×10^5 cells/well) and co-treated with GO/CDDP for 24 h, with or without inhibitor pretreatment. After PBS washes, the cells were fixed and permeabilized as described [10], washed with PBS and incubated with the primary antibody (1:100 dilution) for 1 h at room temperature. The primary antibody was specific for active caspase 3 (ab2302, abcam), HMGB1 (ab18256, abcam), LC3 (LC3B isoform, 3868, Cell Signaling), p62 (H00008878, Abnova) or Lamp-2 (GTX13524, GeneTex). After PBS washes, the cells were incubated with the secondary antibody (1:100 dilution) for 1 h at room temperature in the dark. The secondary antibodies purchased from Jackson ImmunoResearch included Cy3-conjugated goat anti-mouse (for p62) or anti-rat (for Lamp-2) IgG, or Alexa 488 goat anti-rabbit antibody (for LC3, caspase 3 and HMGB1). For LC3 labeling and blue fluorescence emission, Alexa Fluor® 405-conjugated goat anti-rabbit IgG (Invitrogen) was used as the secondary antibody. After washing, the cells were counterstained with 4,6-diamidino-2-phenylindole (DAPI, Vector Labs) and visualized with a confocal microscope. The images were captured and analyzed using Image-Pro Plus 6.0 (Media Cybernetics).

For quantitative analyses, ≈100–150 cells from 3 independent culture experiments were counted for each group. Dividing the number of caspase 3^+ or cytoplasmic HMGB1$^+$ cells by DAPI$^+$ cells yielded the percentages of caspase 3^+ cells or HMGB1 release. The number of cells with LC3/p62 or LC3/Lamp-2 co-localizing in the cytosol was also counted and divided by the number of DAPI$^+$ cells. The cells containing 3 or more LC3 puncta in the nucleus were scored as LC3$^+$. Dividing the number of LC3$^+$ cells by the number of DAPI$^+$ cells yielded the percentage of cells with LC3 puncta in the nucleus.

2.6. Analysis of CDDP concentrations

CT26 cells cultured in 10 cm plates were treated with GO, CDDP or GO/CDDP, trypsinized and lysed in RIPA buffer containing 1% Triton-X 100. Alternatively, the nuclear fraction was separated as described [20]. The Pt concentrations in the whole cell lysates and the nuclear fractions were analyzed by inductively coupled plasma mass spectrometry (ICP-MS, Agilent, 7500ce).

2.7. Animal experiment

Animal experiments were performed in compliance with the Guide for the Care and Use of Laboratory Animals (Ministry of Science and Technology, Taiwan), with the approval of the National Tsing Hua University Institutional Animal Care and Use Committee. Mouse CT26 cells were resuspended in PBS (1×10^6 cells/mL) and injected (5×10^4 cells in 50 μL) subcutaneously into the front of the thigh of BALB/cByJNarl male mice (6 weeks). The tumor volume reached ≈10 mm^3 in 5 days (defined as day 0) and then PBS ($n = 4$), GO (2.5 mg/kg, $n = 4$), CDDP (10 mg/kg, $n = 6$) or GO/CDDP (2.5 mg/kg GO+10 mg/kg CDDP, $n = 6$) was injected intratumorally using the concentrations described previously [14,21,22]. The mice received the second injection again at day 6 and were sacrificed at day 18. Alternatively, the mice were sacrificed at day 5 and the tumors were removed and sectioned.

2.8. Histology and immunohistochemistry

The cryostat sections (5 μm thick) were stained using the Live/Dead viability assay kit (Invitrogen). For immunohistochemical staining, the cryostat sections were fixed in methanol, washed and blocked with the blocking buffer (0.1% Tween 20, 1% bovine serum albumin, 1% goat serum in PBS, pH 7.4) for 30 min, followed by incubation with the primary antibody (1:50 dilution) for 1 h at room temperature. The primary antibodies specific for active caspase 3, HMGB1, L1/calprotectin (for macrophage), CD4, CD8 and CD11c (for DCs) were purchased from abcam. The

primary antibody specific for LC3 was purchased from Cell Signaling. After 3 PBS washes, the sections were incubated with the secondary antibody for 1 h at room temperature in the dark. The secondary antibodies were Alexa 488-conjugated goat anti-rabbit (for HMGB1 and LC3, Jackson ImmunoResearch) or anti-mouse (for CD4, L1/calprotectin and CD11c, Jackson ImmunoResearch) antibody or Cy3-conjugated goat anti-rat IgG (for CD8, Invitrogen). The sections were counterstained with DAPI, examined using the confocal microscope and 7–10 images for each group were quantified using Image-Pro Plus 6.0. Dividing the green or red fluorescence intensity (antigen) by the blue fluorescence intensity (DAPI) yielded the percentages (e.g. the percentage of HMGB1 release).

2.9. Statistical analysis

The quantitative *in vitro* data were statistically analyzed by one-way ANOVA and represented the mean ± standard deviation (s.d.) of at least 3 independent culture experiments. The *in vivo* image analysis data were also analyzed by one-way ANOVA. $p < 0.05$ was considered significant.

3. Results

3.1. Combination of GO and chemotherapy drugs for improved cytotoxicity on colon cancer cell

To explore whether GO enhanced the cytotoxic effects of chemotherapy drugs, we separately treated CT26 cells for 24 h with 4 drugs (CPT-11, DOX, OXA and CDDP) at concentrations that reportedly impart cytotoxicity [14–16]. Without GO co-treatment, CPT-11 (50 μg/mL), DOX (5 μg/mL) and OXA (100 μg/mL) imparted cytotoxicity, as judged from the lower cell density (Fig. 1A) and viability (Fig. 1B) than the untreated control. However, co-treatment with GO at 50 μg/mL (a concentration sufficient to induce autophagy in CT26 cells [11]) and either one of these drugs did not further lower the viability. In contrast, CT26 cells were resistant to CDDP as CDDP (200 μg/mL) alone only decreased the cell viability to 82.0 ± 4.8% (Fig. 1B). However, GO/CDDP co-treatment led to a precipitous decrease of cell viability to 35.0 ± 5.6% (Fig. 1B), indicating that GO (50 μg/mL) and CDDP (200 μg/mL) synergistically enhanced the killing of CT26 cells. The synergistic killing was also observed at low CDDP concentration (25 μg/mL), albeit to a lesser extent (data not shown).

3.2. Combination of GO and CDDP enhanced the necrosis of CT26 cells

To evaluate the death mechanism induced by GO/CDDP, we treated CT26 cells with GO (50 μg/mL), CDDP (200 μg/mL) or co-treated cells with GO/CDDP for 24 h and measured necrosis/apoptosis by Annexin V/7-AAD staining and flow cytometry. Fig. 2A depicts that both GO and CDDP only induced slight necrosis and apoptosis, whereas GO/CDDP resulted in 63.9 ± 4.0% of necrotic cells and 13.3 ± 0.9% of apoptotic cells. Caspase-3 immunostaining and ensuing image analysis attested that GO/CDDP provoked a low percentage (16.1 ± 2.2%) of apoptotic cells (Fig. 2B–C). Furthermore, we performed immunofluorescence microscopy for high mobility group B1 (HMGB1), which is a nuclear protein but is released into cytosol and out of cells after necrosis [14,23–25]. Fig. 2D illustrates that HMGB1 was released into the cytosol or out of cells in the GO/CDDP group (arrows) but was mainly retained in the nuclei in other

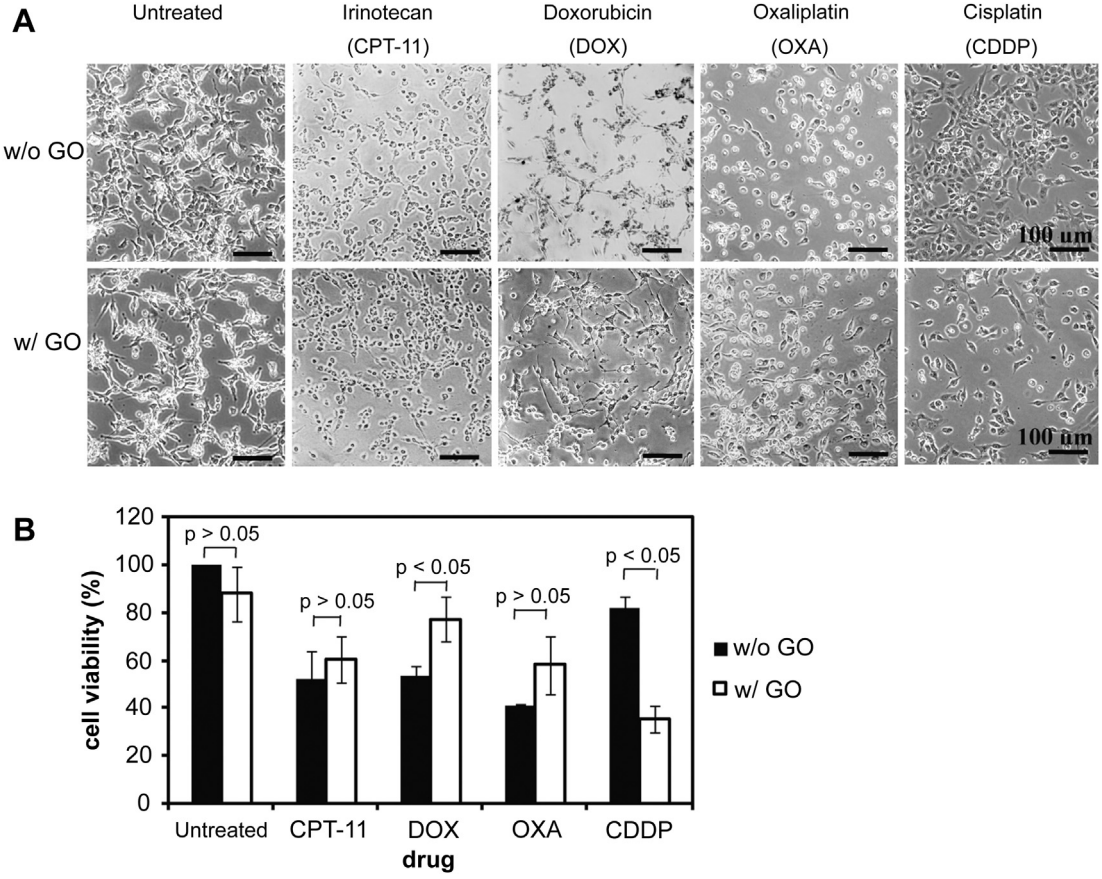

Fig. 1. Combination of GO and chemotherapy drugs for improved killing of CT26 cells. (A) Microscopic observation. (B) Cell viability measured by MTT assay. CT26 cells seeded to 6-well plates (3.0×10^5 cells/well) were cultured overnight, washed with PBS and treated for 24 h in RPMI-1640 medium containing 10% FBS and the chemotherapy drug (50 μg/mL of CPT-11, 5 μg/mL of DOX, 100 μg/mL of OXA or 200 μg/mL of CDDP), with or without 50 μg/mL of GO. Quantitative data represent the mean ± S.D. of at least 3 independent culture experiments.

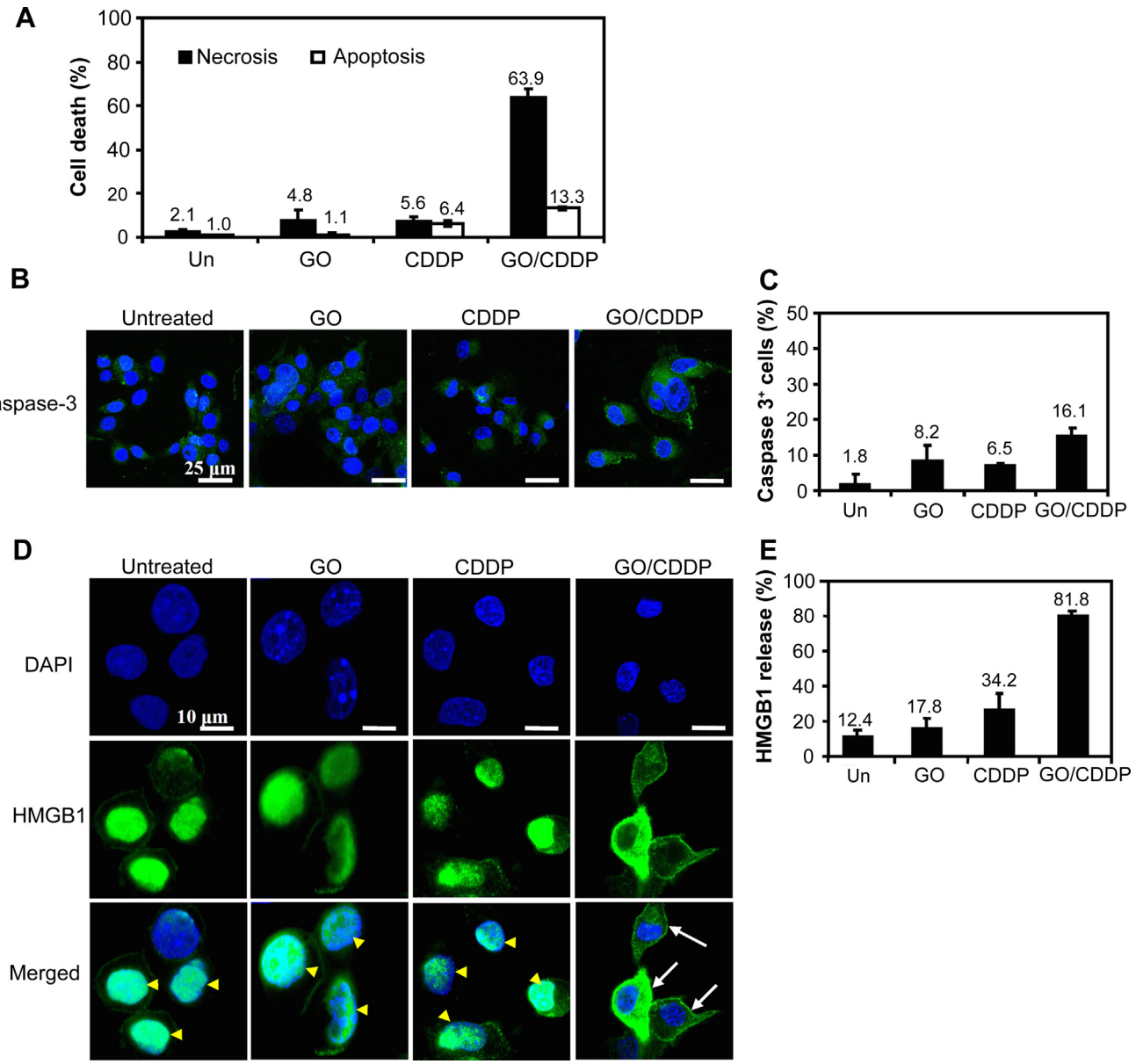

Fig. 2. Combination of GO and CDDP enhanced the necrosis of CT26 cells. CT26 cells were treated with GO (50 μg/mL) alone, CDDP (200 μg/mL) alone or co-treated with GO/CDDP for 24 h and measured for necrosis/apoptosis by Annexin V/7-AAD staining and flow cytometry (A). The cells were subjected to immunofluorescence microscopy and image analysis for active caspase 3 (B and C) and HMGB1 (D and E). For quantitative image analysis, 100–150 cells from 3 independent culture experiments were counted and the percentages of cells with active caspase 3 and HMGB1 release were calculated as described in Materials and methods. Arrowheads indicate the nuclear HMGB1; arrows indicate the HMGB1 released into cytosol.

groups (arrowheads). Image analysis (Fig. 2E) further indicated that up to 81.8 ± 2.7% of cells released HMGB1 into cytosol after GO/CDDP co-treatment. The Western blot (Fig. S1) also indicated that GO/CDDP gave rise to the decrease of RIP1 and increase of RIP3 proteins, a hallmark of necrosis. These data collectively confirmed that necrosis contributed to the GO/CDDP-induced cell death.

3.3. Induction of autophagy and nuclear import of LC3 and CDDP

Since GO at 50 μg/mL induces autophagy [10], we next explored the extent of autophagy by treating CT26 cells as in Fig. 2 and performing immunofluorescence microscopy. As shown in Fig. 3A–B, GO or CDDP triggered co-localization of LC3 puncta and p62 as well as co-localization of LC3 puncta and Lamp-2 in the cytosol (indicated by arrows), which indicate the formation of autophagosomes and autolysosomes, respectively. GO/CDDP also elicited the co-localization of LC3/p62 and LC3/Lamp-2 in the cytosol. Meanwhile, GO, CDDP and GO/CDDP all induced the conversion of LC3-I to LC3-II (Fig. S2). Note, however, that only GO/CDDP additionally evoked evident accumulation of LC3 puncta in the nucleus (Fig. 3A–B) and these LC3 puncta did not co-localize with p62 or Lamp-2 (arrowheads in Fig. 3A–B, Fig. S3).

The image analysis (Fig. 3C) further attested that GO alone led to >60% of cells with $LC3^+$ autophagosomes (top panel) and autolysosomes (middle panel) in the cytosol, but <25% of cells with LC3 puncta in the nucleus (lower panel). Compared to GO, CDDP led to lower percentages of cells with $LC3^+$ autophagosomes and autolysosomes in the cytosol, and <20% of cells with $LC3^+$ puncta in the nucleus (lower panel). GO/CDDP, intriguingly, elicited moderate percentages of cells with $LC3^+$ autophagosomes and autolysosomes

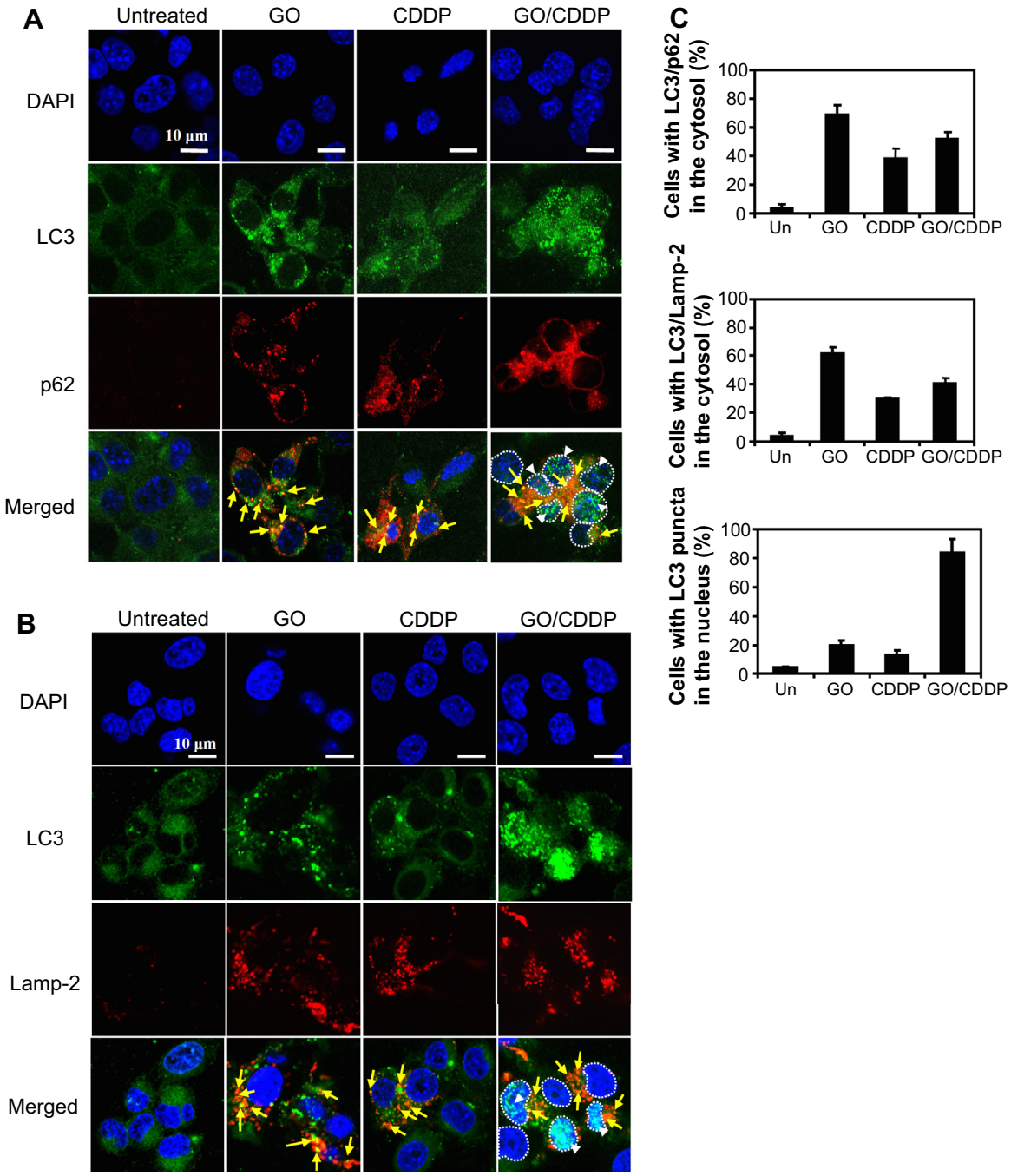

Fig. 3. GO/CDDP induced autophagy and nuclear accumulation of LC3. CT26 cells were treated as in Fig. 2 and subjected to immunofluorescence microscopy for LC3 and p62 (A) or for LC3 and Lamp-2 (B). The cells were counterstained with DAPI. Image analyses were performed to quantify the percentages of cells with LC3/p62 and LC3/Lamp-2 co-localizing in the cytosol as well as the percentages of cells with LC3 puncta in the nucleus (C). Arrows indicate the co-localization of LC3/p62 or LC3/Lamp-2 in the cytosol. Arrowheads indicate the LC3 puncta in the nucleus. For quantitative image analysis, 100–150 cells from 3 independent culture experiments were counted. Cells with 3 or more LC3 puncta were scored as $LC3^{+}$.

in the cytosol, but gave rise to >80% of cells with LC3 puncta in the nucleus (lower panel in Fig. 3C and Fig. S4). Because LC3 is generally considered a cytoplasmic protein [1], these data suggested that GO/CDDP provoked nuclear import of LC3.

To examine whether GO was concomitantly transported to the nucleus upon GO/CDDP treatment, we treated cells with rhodamine 6G-conjugated GO (GO-R6G) alone or together with CDDP (GO-R6G/CDDP), followed by immunolabeling of LC3 with the blue fluorescence-emitting antibody. In the GO-R6G-treated cells (upper panel, Fig. 4A) both LC3 and GO-R6G were mainly localized in the cytosol. In the cells co-treated with GO-R6G/CDDP (lower panel, Fig. 4A), abundant LC3 was translocated to the nucleus whereas GO-R6G remained in the cytosol, indicating that GO/CDDP did not induce the GO transport towards nucleus.

We next explored whether the platinum (Pt)-containing CDDP was transported to the nucleus by treating CT26 cells as in Fig. 3 and analyzing Pt concentrations in the nuclear fraction (Fig. 4B) and cell lysate (Fig. 4C) by inductively coupled plasma mass spectrometry

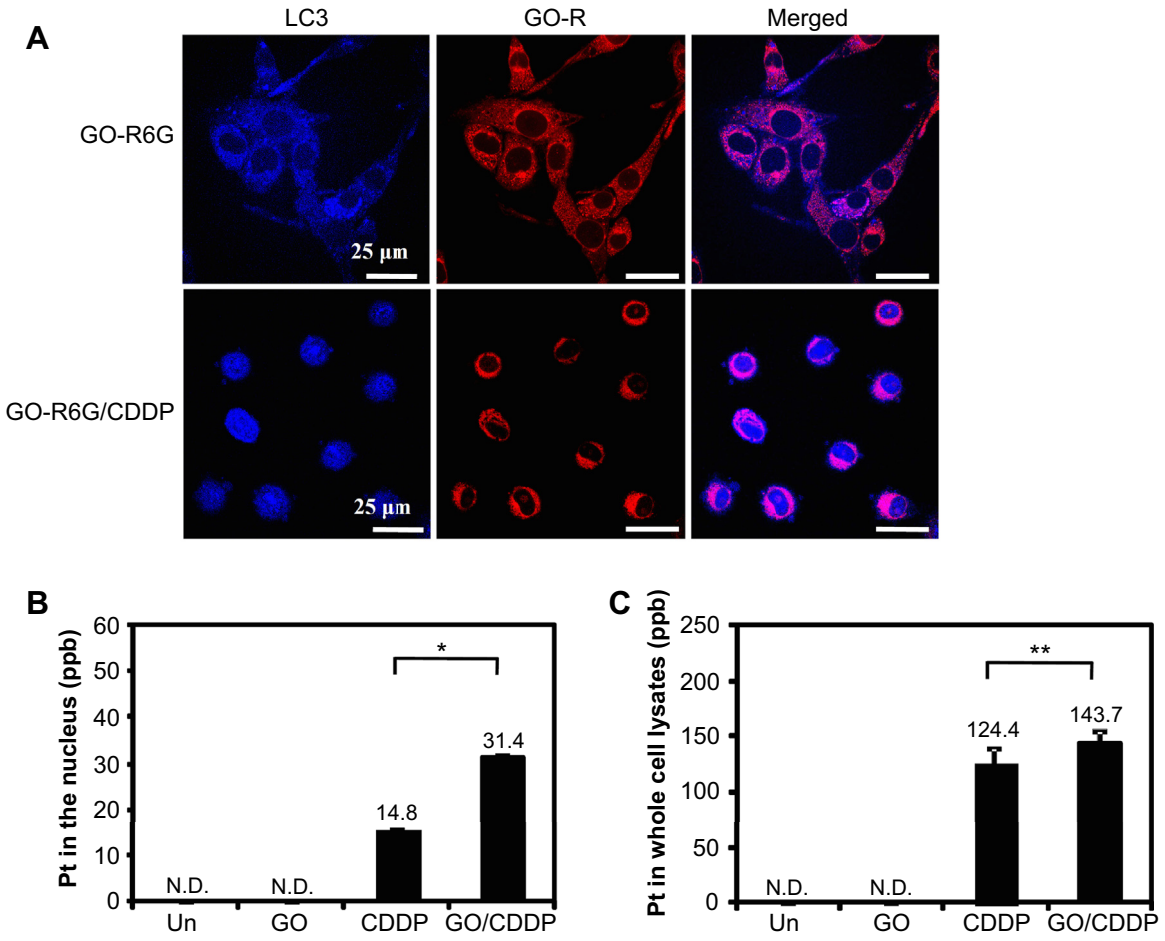

Fig. 4. Nuclear import of GO and CDDP. CT26 cells were treated with GO conjugated with rhodamine 6G (GO-R6G) alone or together with CDDP (GO-R6G/CDDP) for 24 h, followed by immunolabeling of LC3 with the blue fluorescence-emitting antibody Alexa Fluor® 405 (because rhodamine 6G emits red fluorescence that partially overlaps with green fluorescence). The cells were excited at 404 nm and 488 nm to reveal the subcellular location of LC3 and GO-R6G, respectively (A). The Pt concentrations in the nucleus (B) and the whole cell lysates (C) were measured by ICP-MS. Quantitative data represent the mean ± S.D. of 3 independent culture experiments. $^{*}p < 0.05$; $^{**}p > 0.05$; N.D., not detectable.

(ICP-MS). As shown, the nuclear Pt concentration was only 14.8 ± 0.2 ppb in the CDDP-treated cells, but was significantly ($p < 0.05$) elevated to 31.4 ± 0.1 ppb in the GO/CDDP-treated cells (Fig. 4B), indicating that GO/CDDP improved the nuclear import of CDDP. Conversely, the Pt concentrations were statistically similar ($p > 0.05$) in the whole lysates of the CDDP- and GO/CDDP-treated cells (Fig. 4C), suggesting that GO/CDDP did not enhance the overall CDDP uptake into the cells.

3.4. Essential events for nuclear import and necrosis

To elucidate the events essential for the enhanced nuclear transport, we treated the cells with the inhibitors of phagophore formation (3-methyladenine, 3-MA), autolysosome formation (bafilomycin A1, BafA1) or importin-α/β (ivermectin, IVM [26]), followed by GO/CDDP co-treatment. The immunofluorescence microscopy (Fig. 5A) and image analysis (Fig. 5B) demonstrated that GO/CDDP treatment without any inhibitor (Control) still induced the nuclear transport of LC3. BafA1 pretreatment hindered LC3/p62 and LC3/Lamp-2 co-localization, indicating the inhibition of autophagy, but BafA1 did not significantly ($p > 0.05$) abrogate the nuclear translocation of LC3, as 65.0 ± 14.1% of BafA1-treated cells contained LC3 dots in the nucleus. Conversely, 3-MA treatment remarkably inhibited the formation of LC3 puncta and ensuing nuclear import, as the percentage of cells containing nuclear LC3 dropped to 17.5 ± 3.5%. IVM treatment still allowed for the co-localization of LC3/p62 and LC3/Lamp-2 in the cytosol (Fig. 5A), but reduced the percentage of cells containing nuclear LC3 to 12.5 ± 3.5% (Fig. 5B), indicating that inhibiting importin-α/β did not completely abolish autophagy but suppressed the nuclear import of LC3.

Meanwhile, the ICP-MS analysis (Fig. 5C) delineated similar nuclear Pt concentrations in the BafA1 (44.7 ± 8.7 ppb) and the Control (40.1 ± 4.6 ppb) groups. However, treatment with 3-MA or IVM significantly lowered the nuclear Pt concentrations to 26.3 ± 6.0 and 31.5 ± 5.7 ppb, respectively.

Since GO/CDDP substantially enhanced the CT26 necrosis (Fig. 2), we next assessed whether the necrosis was correlated with the nuclear import. The bright field observation and HMGB1 staining (Fig. 5D) revealed that 3-MA or IVM, similar to the necrosis inhibitor necrostatin 1 (Nec-1), alleviated the cytotoxicity and mitigated the HMGB1 release to the cytosol. Fig. 5E further showed that 3-MA and IVM significantly attenuated the GO/CDDP-induced necrosis when compared with the Control and BafA1. Fig. 5 altogether confirms that inhibiting the phagophore formation by 3-MA and suppressing importin-α/β by IVM abolished the nuclear import of LC3/CDDP and the GO/CDDP-induced necrosis. However, suppressing autolysosome formation by BafA1 neither remarkably impeded the LC3/CDDP nuclear transport nor tremendously attenuated necrosis.

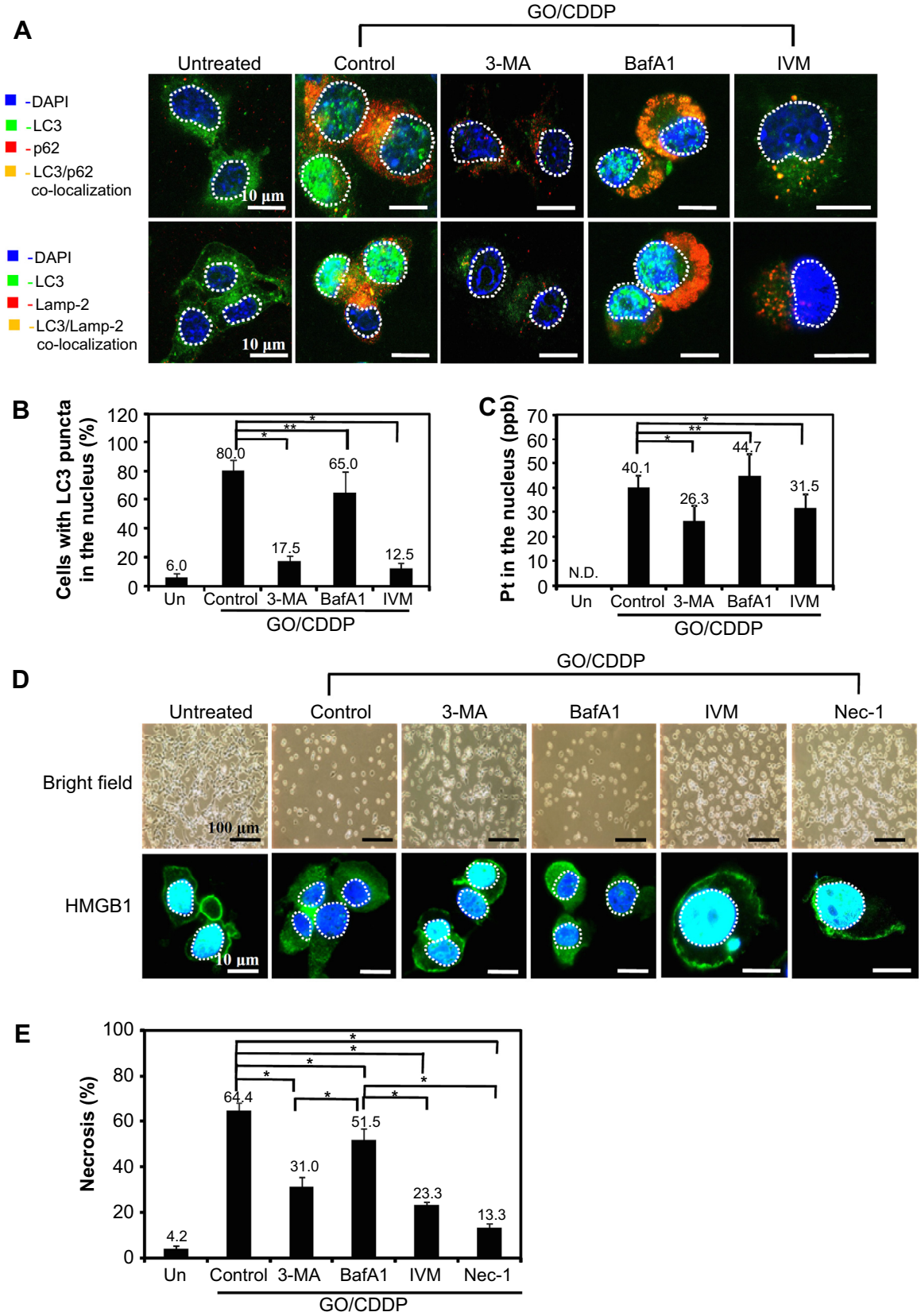

Fig. 5. Essential events for nuclear import and necrosis. CT26 cells were treated without inhibitor (Control) or with 3-MA, BafA1 or IVM, followed by GO/CDDP co-treatment for 24 h. The cells were subjected to immunofluorescence microscopy for LC3/p62 or LC3/Lamp-2 (A), image analysis (B) and ICP-MS measurement of Pt concentration in the nucleus (C). For image analysis, 100–150 cells from 3 independent culture experiments were counted. Yellow dots indicate the co-localization of LC3/p62 or LC3/Lamp-2. Cells with 3 or more LC3 puncta were scored as $LC3^{+}$. Additionally, the cells were pre-treated with Nec-1 for 1 h as a control. The cells were observed under the light microscope or subjected to immunofluorescence microscopy for HMGB1 (D). The percentages of necrotic cells were also measured (E). $^{*}p < 0.05$; $^{**}p > 0.05$. (For interpretation of the references to color in this figure legend, the reader is referred to the web version of this article.)

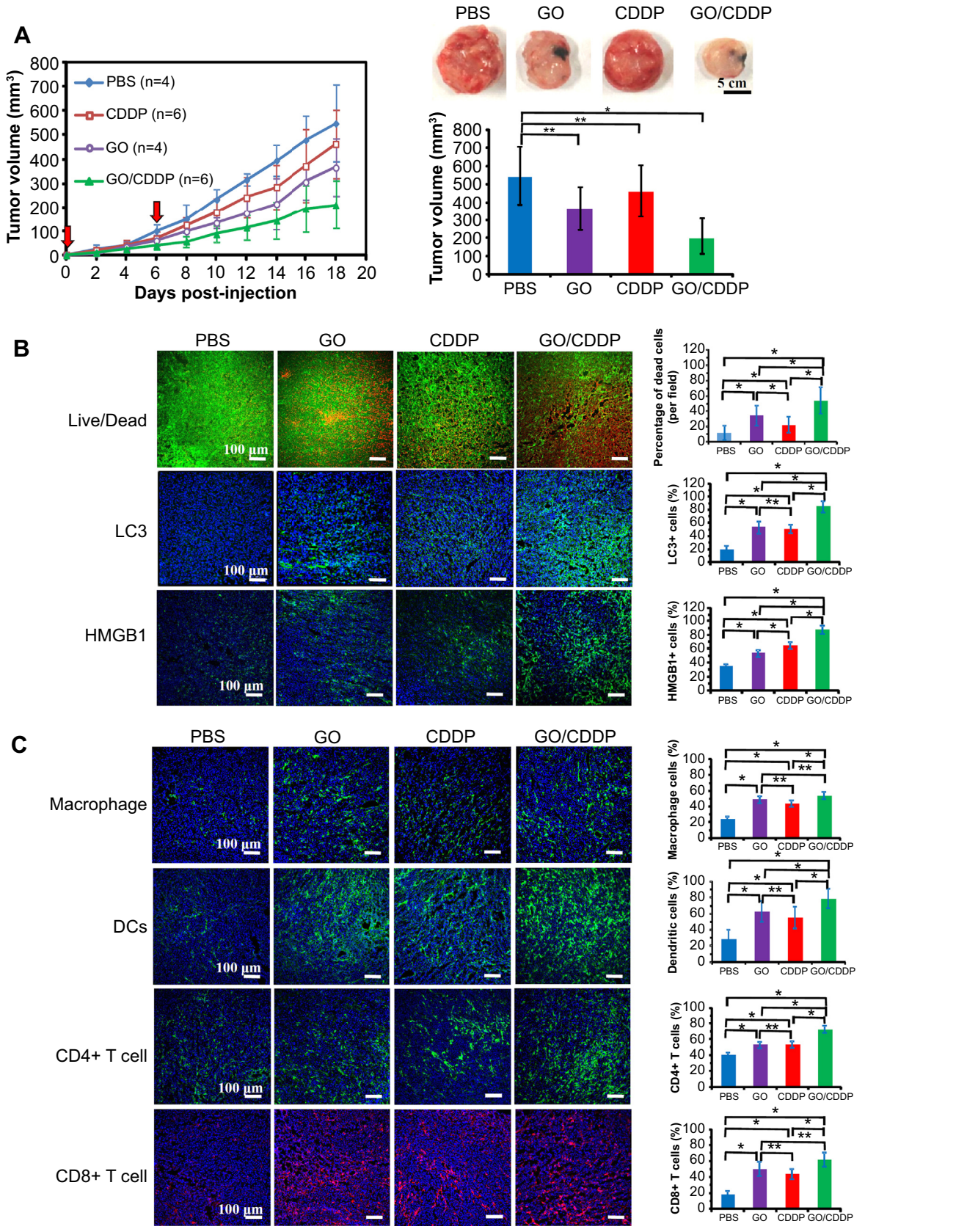

Fig. 6. GO/CDDP injection inhibited CT26 tumor growth and enhanced the cell death, autophagy, HMGB1 release and immune cell infiltration. (A) Tumor volume and appearance. (B) Live/Dead analysis and immunostaining for LC3 and HMGB1. (C) Immunostaining for macrophage, DCs, $CD4^+$ and $CD8^+$ T cells. CT26 cells (5×10^4 cells) were injected subcutaneously into BALB/c mice and developed into tumors with volume reaching 10 mm^3 in 5 days (defined as day 0). The mice received intratumoral injection of PBS ($n = 4$), GO ($n = 4$), CDDP ($n = 6$) or GO/CDDP ($n = 6$) at day 0 and another injection at day 6. Alternatively, the experiments were repeated and tumors were removed after sacrifice of mice at day 5. The tumors sections were subjected to Live/Dead assays or immunohistochemical staining. Image analysis and calculation of percentages of cells were performed as described in Materials and methods. The images are representative of sections from 4 animals. $^*p < 0.05$; $^{**}p > 0.05$.

3.5. Combination of GO and CDDP synergistically enhanced antitumor effects

We next evaluated the potential of GO/CDDP in colon cancer therapy by injecting CT26 cells subcutaneously into BALB/c mice, followed by intratumoral injections of PBS ($n = 4$), CDDP ($n = 6$), GO ($n = 4$) or GO/CDDP ($n = 6$) at day 0 (when the tumor volume reached ≈ 10 mm^3) and day 6. In comparison with PBS, both GO and CDDP slightly decelerated the tumor growth (left panel, Fig. 6A) although the tumor volume at day 18 (right panel, Fig. 6A) was not significantly smaller than that of the PBS group. Nonetheless, GO/CDDP resulted in slower tumor growth and significantly ($p < 0.05$) smaller tumor (212 ± 98 mm^3 at day 18) than PBS, without compromising the body weight (Fig. S5).

For histology assessment, we repeated the aforementioned experiment and removed the tumors at day 5 for sectioning and analysis. As confirmed by Live/Dead assays as well as the LC3 and HMGB1 immunostaining/quantitative analyses (Fig. 6B), GO alone and CDDP alone induced significantly ($p < 0.05$) more pronounced cell death, autophagy and necrosis than PBS. Furthermore, the GO/CDDP group elicited significantly ($p < 0.05$) higher degrees of cell death, autophagy and necrosis than all other groups.

Compared with PBS, both GO and CDDP significantly ($p < 0.05$) stimulated the infiltration of macrophage, dendritic cells (DCs), $CD4^+$ and $CD8^+$ T cells into the tumor bed, albeit the lack of statistical significance between the GO and CDDP groups (Fig. 6C). GO/CDDP also evoked the infiltration of immune cells and significantly excelled in the infiltration of DCs and $CD4^+$ T cells when compared with GO alone and CDDP alone (Fig. 6C).

4. Discussion

Chemoresistance is one major obstacle to the success of chemotherapy and is commonly attributed to the inability of cancer cells to die by apoptosis. The development of anticancer modalities that can induce other forms of cell death is therefore desired for cancer therapy [27]. One overriding objective of this study was to evaluate the potential of GO as a chemosensitizer. Among the 4 drugs, we uncovered that GO can sensitize the CDDP-mediated killing of CDDP-resistant CT26 cells (Fig. 1). Of note, GO and CDDP alone only elicited low degrees of apoptosis and necrosis (Fig. 2) despite the induction of autophagy (Fig. 3), suggesting that GO and CDDP alone did not evoke evident autophagy-associated death in CT26 cells. In contrast, GO/CDDP-induced moderate levels of autophagic flux (Fig. 3), but substantially potentiated the nuclear import of LC3 (Fig. 3) and CDDP (Fig. 4) and enhanced the necrosis (Fig. 2), without provoking the nuclear import of GO (Fig. 4). Neither did the nuclear LC3 co-localize with the lysosomal membrane protein Lamp-2 (Figs. 3 and 5), nor blocking autolysosome formation significantly inhibited the nuclear import of LC3/CDDP and alleviated cell necrosis (Fig. 5), indicating that autolysosome formation (hence the completion of autophagic flux) was dispensable for the nuclear trafficking of LC3/CDDP and necrosis.

Conversely, treatment with 3-MA significantly impaired the nuclear import of LC3/CDDP and alleviated the necrosis (Fig. 5). Because 3-MA inhibits class I and class III PtdIns3Ks and hence phagophore-mediated sequestration [28], the phagophore formation appeared to be crucial for the LC3 nuclear import. However, the nuclear LC3 did not co-localize with p62 (Figs. 3 and 5), suggesting that tethering of p62 to LC3 on the elongating phagophore was dispensable. Meanwhile, IVM suppression of importin-α/β, which is essential for nuclear import of many molecules [29], mitigated the nuclear import of LC3/CDDP and ablated the necrosis (Fig. 5), thereby underscoring the importance of importin-associated nuclear import in the GO/CDDP-induced necrosis. These data altogether suggested that, in addition to the complete autophagic flux, GO/CDDP resulted in diversion of the LC3-containing phagophore from engaging with p62. The diverted LC3 flux was directed towards the nucleus in a way dependent on importin-α/β, which occurred concomitantly with the CDDP nuclear import and necrosis (Fig. S6).

These findings arouse several intriguing questions. First, autophagy has long been considered an event occurring in the cytosol, then how was LC3 transported into the nucleus after GO/CDDP co-treatment? In this regard, in fact some researchers have observed the presence of LC3 in the nucleus [30–33] despite the lack of follow-up investigations. It was also unveiled that LC3 can shuttle between the cytosol and nucleoplasm in COS-7 cells [34]. However, the mechanisms and physiological roles of the LC3 nuclear transport remain unknown. Nonetheless, LC3 can be incorporated into intracellular protein aggregates [33] and exposure of cells (e.g. NIH-3T3) to growth factor increases the interaction of extracellular signal regulated kinase (ERK) cascade components with autophagy proteins such as LC3 in the cytosol and nucleus [35]. These autophagy proteins might have formed pre-autophagosomal structures and interacted with ERK2 to regulate the ERK phosphorylation [35]. In light of these notions and the finding that the GO entry into CT26 cells elicits TLR4 and TLR9 responses [11], which signal through the nuclear translocation of transcription factors, we propose that, in addition to the LC3 destined to autolysosomes, GO/CDDP co-treatment provoked the interaction of LC3 with other proteins (e.g. transcription factors or signaling complexes) and re-routed the LC3 flux towards nucleus with the aid of importin-α/β.

Second, why did GO/CDDP concomitantly enhance CDDP delivery into the nucleus? CDDP can be taken up into cells by passive diffusion and copper transporters and acts on genomic DNA to induce cell death, but little is known about its nuclear import pathway [36,37]. Yet it is known that only ≈ 1–5% of intracellular CDDP binds to DNA [36,37] and the remaining 75–85% of CDDP is associated with other molecules such as metallothionein/glutathione [36], microfilaments and proteins [38]. Of note, CDDP can be transported to lysosomes for degradation [39,40] and autophagy may play roles in this delivery route [41,42]. As such, it is tempting to speculate that CDDP-induced autophagy resulted in the CDDP delivery into lysosomes for degradation, which at least partly accounted for the resistance. GO/CDDP treatment might have diverted the autophagic flux and hence reduced the autophagy-mediated CDDP accumulation in the lysosome, thereby enabling the delivery of more CDDP into the nucleus.

Third, why did GO/CDDP trigger necrosis, instead of apoptosis, as the major form of cell death? For a long time, the antineoplastic effects of CDDP have been ascribed to its ability to generate DNA lesions, hence inducing either senescence or apoptosis [36,37]. However, lines of evidence have shown that CDDP triggers not only apoptosis but also necrosis [43], especially in cancer cells resistant to chemotherapy drugs [37,44]. The cytotoxic effects of CDDP also arise from both nuclear and cytoplasmic signaling pathways [40]. Although the molecular mechanisms that underlie the cytotoxic potential of cytoplasmic CDDP remain poorly understood, it was likely that the enhanced nuclear import of CDDP altered the distribution of CDDP in the cytosol and nucleus, leading to the switch of death mechanisms. Meanwhile, GO treatment of macrophages induces programmed necrosis in a TLR4 signaling-dependent manner [45]. Since GO triggers the TLR4 responses in CT26 cells [11], the TLR4 responses might have orchestrated with the CDDP-induced responses to promote necrosis of CT26 cells.

In vivo, antineoplastic chemotherapies are particularly efficient when they elicit immunogenic cell death, which is mediated by damage-associated molecular patterns (DAMPs) such as

the exposure of calreticulin (CRT) on the cell surface, release of HMGB1 and secretion of adenosine triphosphate (ATP) [46]. The binding of these DAMPs to receptors on the DCs triggers host immune responses and promotes the antitumor effects [46]. However, not all chemotherapeutic agents can effectively induce active emission of DAMPs by dying tumor cells [47]. For instance, in the murine colon cancer models CDDP fails to elicit CRT exposure and immunogenic cell death, which contributes to the colon cancer resistance to CDDP [14]. In accord with this notion, CDDP only conferred marginal antitumor effects (Fig. 6A–B).

Conversely, autophagy is essential for the immunogenic release of ATP from dying tumor cells and the recruitment of DCs and T lymphocytes into the CT26-derived colon cancer bed after chemotherapy [48]. GO/CDDP provoked potent autophagy, triggered more pronounced cell death and HMGB1 release than GO and CDDP *in vitro* (Fig. 2) and *in vivo* (Fig. 6B), suggesting that GO/CDDP was able to improve the release of DAMPs to potentiate the host immune response (e.g. immune cell infiltration). Furthermore, GO induced autophagy and TLR4 signaling upon exposure to CT26 cells [11] and macrophages [10]. As such, one may envisage that GO injection into the CT26 tumors not only acted on the tumor cells, but also activated macrophages and TLR4 signaling, thereby further enhancing host immune responses and imparting adjuvant effects. These factors collectively contributed to the enhanced infiltration of macrophages and $CD4^+$ helper T cells into the tumor bed and synergistic antitumor effects by GO/CDDP (Fig. 6A and C).

5. Conclusions

We uncovered that GO in combination with CDDP enhanced the nuclear import of LC3 and CDDP, potentiated the necrosis of CT26 cells *in vitro* and synergistically substantiated the antineoplastic effects in mice bearing the CT26 colon tumor. This study unveiled a new mechanism (enhanced nuclear import of chemotherapy drug) accounting for how nanomaterials may sensitize chemoresistant cancer cells. Although whether this mechanism is applicable to different nanomaterials, drugs and cancer types remains to be established, we found that GO/CDDP chemosensitized ovarian cancer cell SKOV3 and cervical cancer cell HeLa as well, although GO/CDDP did not enhance the killing of lung carcinoma cell A549 (Fig. S7). Therefore, this study may pave a new avenue to using GO as a chemosensitizer for the treatment of several cancers. It should be noted, however, that the size of GO may affect the cellular responses it elicited [49], caution should be used when preparing for the GO nanosheets and interpreting the data. Finally, the use of novel combinations of 'old' drugs for new indications has garnered significant interest [50]. CDDP is one of the most common chemotherapy drugs for a wide variety of cancers [36,44], but colorectal and non-small cell lung cancers have intrinsic resistance to CDDP [44]. The combination of GO and CDDP may lead to the revival of CDDP in colon cancer therapy, thereby offering another chemotherapeutic regimen.

Acknowledgments

The authors acknowledge the support from the National Tsing Hua University (Toward World-Class University Project 102N2051E1, 103N2051E1 and NTHU-CGMH Joint Research Program 103N2758E1) and Ministry of Science and Technology (NSC 102-2622-E-007-022-CC1, NSC 102-2221-E-007-023-MY3 and MOST 103-2221-E-007-093-MY3), Taiwan.

Appendix A. Supplementary data

Supplementary data related to this article can be found at http://dx.doi.org/10.1016/j.biomaterials.2014.11.034.

References

[1] Levine B, Mizushima N, Virgin HW. Autophagy in immunity and inflammation. Nature 2011;469:323–35.
[2] Yang ZJ, Chee CE, Huang S, Sinicrope FA. The role of autophagy in cancer: therapeutic implications. Mol Cancer Ther 2011;10:1533–41.
[3] Fullgrabe J, Klionsky DJ, Joseph B. The return of the nucleus: transcriptional and epigenetic control of autophagy. Nat Rev Mol Cell Biol 2014;15:65–74.
[4] Gewirtz DA. The four faces of autophagy: implications for cancer therapy. Cancer Res 2014;74:647–51.
[5] Chen GY, Pang DWP, Hwang SM, Tuan HY, Hu YC. A graphene-based platform for induced pluripotent stem cells culture and differentiation. Biomaterials 2012;33:418–27.
[6] Zhang L, Lu Z, Zhao Q, Huang J, Shen H, Zhang Z. Enhanced chemotherapy efficacy by sequential delivery of siRNA and anticancer drugs using PEI-grafted graphene oxide. Small 2011;7:460–4.
[7] Zhang L, Xia J, Zhao Q, Liu L, Zhang Z. Functional graphene oxide as a nanocarrier for controlled loading and targeted delivery of mixed anticancer drugs. Small 2010;6:537–44.
[8] Yang K, Wan J, Zhang S, Tian B, Zhang Y, Liu Z. The influence of surface chemistry and size of nanoscale graphene oxide on photothermal therapy of cancer using ultra-low laser power. Biomaterials 2012;33:2206–14.
[9] Tao Y, Ju E, Ren J, Qu X. Immunostimulatory oligonucleotides-loaded cationic graphene oxide with photothermally enhanced immunogenicity for photothermal/immune cancer therapy. Biomaterials 2014;35:9963–71.
[10] Chen G-Y, Yang H-J, Lu C-H, Chao Y-C, Hwang S-M, Chen C-L, et al. Simultaneous induction of autophagy and toll-like receptor signaling pathways by graphene oxide. Biomaterials 2012;33:6559–69.
[11] Chen GY, Chen CL, Tuan HY, Yuan PX, Li KC, Yang HJ, et al. Graphene oxide triggers toll-like receptors/autophagy responses in vitro and inhibits tumor growth in vivo. Adv Healthc Mater 2014;3:1486–95.
[12] Tournigand C, Andre T, Bonnetain F, Chibaudel B, Lledo G, Hickish T, et al. Adjuvant therapy with fluorouracil and oxaliplatin in stage II and elderly patients (between ages 70 and 75 years) with colon cancer: subgroup analyses of the Multicenter International Study of Oxaliplatin, Fluorouracil, and Leucovorin in the Adjuvant Treatment of Colon Cancer trial. J Clin Oncol 2012;30:3353–60.
[13] Choi CK, Chan RT, Tung SY, Lui L, Siu S, Au GK, et al. Efficacy of combination chemotherapy with irinotecan (CPT-11) plus capecitabine in patients with metastatic or advanced colorectal carcinoma–a dual-centre phase II study: the MAC-6. Clin Oncol (R Coll Radiol) 2008;20:168–75.
[14] Tesniere A, Schlemmer F, Boige V, Kepp O, Martins I, Ghiringhelli F, et al. Immunogenic death of colon cancer cells treated with oxaliplatin. Oncogene 2010;29:482–91.
[15] Tyedmers J, Mogk A, Bukau B. Cellular strategies for controlling protein aggregation. Nat Rev Mol Cell Biol 2010;11:777–88.
[16] Peracchio C, Alabiso O, Valente G, Isidoro C. Involvement of autophagy in ovarian cancer: a working hypothesis. J Ovarian Res 2012;5:22.
[17] Zhang Q, Yang W, Man N, Zheng F, Shen Y, Sun K, et al. Autophagy-mediated chemosensitization in cancer cells by fullerene C60 nanocrystal. Autophagy 2009;5:1107–17.
[18] Wang X, Zhong SH, He Y, Song GW. A graphene oxide-rhodamine 6G nanocomposite as turn-on fluorescence probe for selective detection of DNA. Anal Methods 2012;4:360–2.
[19] Yang HP, Hu HL, Ni ZH, Poh CK, Cong CX, Lin JY, et al. Comparison of surface-enhanced Raman scattering on graphene oxide, reduced graphene oxide and graphene surfaces. Carbon 2013;62:422–9.
[20] Wan B, Wang ZX, Lv QY, Dong PX, Zhao LX, Yang Y, et al. Single-walled carbon nanotubes and graphene oxides induce autophagosome accumulation and lysosome impairment in primarily cultured murine peritoneal macrophages. Toxicol Lett 2013;221:118–27.
[21] Uchino H, Matsumura Y, Negishi T, Koizumi F, Hayashi T, Honda T, et al. Cisplatin-incorporating polymeric micelles (NC-6004) can reduce nephrotoxicity and neurotoxicity of cisplatin in rats. Br J Cancer 2005;93:678–87.
[22] Zhang H, Zhang S, He H, Zhao W, Ren K, Chen J, et al. RasGAP-derived peptide 38GAP potentiates the cytotoxicity of cisplatin through inhibitions of Akt, ERK and NF-kappaB in colon carcinoma HCT116 cells. Cancer Lett 2011;308:62–70.
[23] Yang HN, Rivera Z, Jube S, Nasu M, Bertino P, Goparaju C, et al. Programmed necrosis induced by asbestos in human mesothelial cells causes high-mobility group box 1 protein release and resultant inflammation. Proc Natl Acad Sci 2010;107:12611–6.
[24] Eisenberg T, Knauer H, Schauer A, Buttner S, Ruckenstuhl C, Carmona-Gutierrez D, et al. Induction of autophagy by spermidine promotes longevity. Nat Cell Biol 2009;11:1305–14.
[25] Raucci A, Palumbo R, Bianchi ME. HMGB1: a signal of necrosis. Autoimmunity 2007;40:285–9.

[26] Wagstaff KM, Sivakumaran H, Heaton SM, Harrich D, Jans DA. Ivermectin is a specific inhibitor of importin alpha/beta-mediated nuclear import able to inhibit replication of HIV-1 and dengue virus. Biochem J 2012;443:851–6.
[27] Cloonan SM, Williams DC. The antidepressants maprotiline and fluoxetine induce Type II autophagic cell death in drug-resistant Burkitt's lymphoma. Int J Cancer 2011;128:1712–23.
[28] Klionsky DJ, Abdalla FC, Abeliovich H, Abraham RT, Acevedo-Arozena A, Adeli K, et al. Guidelines for the use and interpretation of assays for monitoring autophagy. Autophagy 2012;8:445–544.
[29] Badding MA, Lapek JD, Friedman AE, Dean DA. Proteomic and functional analyses of protein-DNA complexes during gene transfer. Mol Ther 2013;21:775–85.
[30] Bampton ETW, Goemans CG, Niranjan D, Mizushima N, Tolkovsky AM. The dynamics of autophagy visualized in live cells – from autophagosome formation to fusion with endo/lysosomes. Autophagy 2005;1:23–36.
[31] Cieehomska IA, Tolkovsky AM. Non-autophagic GFP-LC3 puncta induced by saponin and other detergents. Autophagy 2007;3:586–90.
[32] Kochl R, Hu XW, Chan EY, Tooze SA. Microtubules facilitate autophagosome formation and fusion of autophagosomes with endosomes. Traffic 2006;7:129–45.
[33] Kuma A, Matsui M, Mizushima N. LC3, an autophagosome marker, can be incorporated into protein aggregates independent of autophagy. Autophagy 2007;3:323–8.
[34] Drake KR, Kang M, Kenworthy AK. Nucleocytoplasmic distribution and dynamics of the autophagosome marker EGFP-LC3. Plos One 2010;5:e9806.
[35] Martinez-Lopez N, Athonvarangkul D, Mishall P, Sahu S, Singh R. Autophagy proteins regulate ERK phosphorylation. Nat Commun 2013;4:2799.
[36] Florea A-M, Büsselberg D. Cisplatin as an anti-tumor drug: cellular mechanisms of activity, drug resistance and induced side effects. Cancers 2011;3:1351–71.
[37] Galluzzi L, Vitale I, Michels J, Brenner C, Szabadkai G, Harel-Bellan A, et al. Systems biology of cisplatin resistance: past, present and future. Cell Death Dis 2014;5:e1257.
[38] Akaboshi M, Kawai K, Ujeno Y, Takada S, Miyahara T. Binding characteristics of (-)-(R)-2-aminomethylpyrrolidine(1,1-cyclobutanedicarboxylato)-2-platinum(II) to DNA, RNA and protein molecules in HeLa cells and its lethal effect: comparison with cis- and trans-diamminedichloroplatinums(II). Jpn J Cancer Res 1994;85:106–11.
[39] Safaei R, Larson BJ, Cheng TC, Gibson MA, Otani S, Naerdemann W, et al. Abnormal lysosomal trafficking and enhanced exosomal export of cisplatin in drug-resistant human ovarian carcinoma cells. Mol Cancer Ther 2005;4:1595–604.
[40] Sancho-Martínez SM, Prieto-García L, Prieto M, López-Novoa JM, López-Hernández FJ. Subcellular targets of cisplatin cytotoxicity: an integrated view. Pharmacol Ther 2012;136:35–55.
[41] Yu H, Su J, Xu Y, Kang JS, Li HY, Zhang L, et al. p62/SQSTM1 involved in cisplatin resistance in human ovarian cancer cells by clearing ubiquitinated proteins. Eur J Cancer 2011;47:1585–94.
[42] Ren JH, He WS, Nong L, Zhu QY, Hu K, Zhang RG, et al. Acquired cisplatin resistance in human lung adenocarcinoma cells is associated with enhanced autophagy. Cancer Biother Radiopharm 2010;25:75–80.
[43] Gonzalez VM, Fuertes MA, Alonso C, Perez JM. Is cisplatin-induced cell death always produced by apoptosis? Mol Pharmacol 2001;59:657–63.
[44] Cepeda V, Fuertes MA, Castilla J, Alonso C, Quevedo C, Perez JM. Biochemical mechanisms of cisplatin cytotoxicity. Anticancer Agents Med Chem 2007;7:3–18.
[45] Qu G, Liu S, Zhang S, Wang L, Wang X, Sun B, et al. Graphene oxide induces toll-like receptor 4 (TLR4)-dependent necrosis in macrophages. ACS Nano 2013;7:5732–45.
[46] Krysko DV, Garg AD, Kaczmarek A, Krysko O, Agostinis P, Vandenabeele P. Immunogenic cell death and DAMPs in cancer therapy. Nat Rev Cancer 2012;12:860–75.
[47] Garg AD, Krysko DV, Verfaillie T, Kaczmarek A, Ferreira GB, Marysael T, et al. A novel pathway combining calreticulin exposure and ATP secretion in immunogenic cancer cell death. EMBO J 2012;31:1062–79.
[48] Michaud M, Martins I, Sukkurwala AQ, Adjemian S, Ma Y, Pellegatti P, et al. Autophagy-dependent anticancer immune responses induced by chemotherapeutic agents in mice. Science 2011;334:1573–7.
[49] Yue H, Wei W, Yue Z, Wang B, Luo N, Gao Y, et al. The role of the lateral dimension of graphene oxide in the regulation of cellular responses. Biomaterials 2012;33:4013–21.
[50] Zong D, Haag P, Yakymovych I, Lewensohn R, Viktorsson K. Chemosensitization by phenothiazines in human lung cancer cells: impaired resolution of γH2AX and increased oxidative stress elicit apoptosis associated with lysosomal expansion and intense vacuolation. Cell Death Dis 2011;2:e181.